

Trigonometric Parallaxes for Two Late-Type Subdwarfs: LSR1425+71 (sdM8.0) and the Binary LSR1610–00 (sd?M6pec)

Conard C. Dahn, Hugh C. Harris, Stephen E. Levine, Trudy Tilleman,
Alice K. B. Monet, Ronald C. Stone,¹ Harry H. Guetter, Blaise Canzian,²
Jeffrey R. Pier

*US Naval Observatory, Flagstaff Station, 10391 West Naval Observatory Road,
Flagstaff, AZ 86001-8521*

dahn@nofs.navy.mil

William I. Hartkopf

US Naval Observatory, 3450 Massachusetts Ave., N.W., Washington, DC 20392-5420

wih@usno.navy.mil

James Liebert

Steward Observatory, University of Arizona, 933 North Cherry Ave., Tucson AZ 85721

liebert@jayhawk.as.arizona.edu

Michael Cushing

Institute for Astronomy, 2680 Woodlawn Drive, Honolulu, HI 96822

mcushing@ifa.hawaii.edu

ABSTRACT

Trigonometric parallax astrometry and BVI photometry are presented for two late-type subdwarf candidates, LSR1425+71 (sdM8.0) and LSR1610–00 (sd?M6pec). For the former we measure an absolute parallax of 13.37 ± 0.51

¹Deceased 10 Sept. 2005

²Current address: L-3 Communications/Brashear, 615 Epsilon Drive, Pittsburgh, PA 15238

mas yielding $M_V = 15.25 \pm 0.09$. The astrometry for LSR1610–00 shows that this object is an astrometric binary with a period of 1.66 ± 0.01 yr. The photocentric orbit is derived from the data; it has a moderate eccentricity ($e \approx 0.44 \pm 0.02$) and a semi-major axis of 0.28 ± 0.01 AU based on our measured absolute parallax of 31.02 ± 0.26 mas. Our radial velocity measure of -108.1 ± 1.6 km s $^{-1}$ for LSR1610–00 at epoch 2006.179, when coupled with the observation of -95 ± 1 km s $^{-1}$ at epoch 2005.167 by Reiners & Basri, indicates a systemic radial velocity of -101 ± 1 km s $^{-1}$ for the LSR1610–00AB pair. The galactic velocity components for LSR1425+71 and LSR1610–00AB – (U, V, W) = $(84 \pm 6, -202 \pm 13, 66 \pm 14)$ km s $^{-1}$ and (U, V, W) = $(36 \pm 2, -232 \pm 2, -61 \pm 2)$ km s $^{-1}$, respectively. For both stars, the velocities are characteristic of halo population kinematics. However, modelling shows that both stars have orbits around the galaxy with high eccentricity that pass remarkably close to the galactic center. LSR1425+71 has a luminosity and colors consistent with its metal-poor subdwarf spectral classification, while LSR1610–00 has a luminosity and most colors indicative of being only mildly metal-poor, plus a uniquely red $B - V$ color. The companion to LSR1610–00 must be a low-mass, substellar brown dwarf. We speculate on the paradoxical nature of LSR1610–00 and possible sources of its peculiarities.

Subject headings: stars: binary — stars: individual (LSR1425+7102, LSR1610-0040) — stars: low-mass — stars: subdwarfs

1. Introduction

Over the last decade, spectroscopic surveys targeting faint stars with large proper motions have identified many subdwarfs with M spectral types. These surveys generally make use of the spectral classification scheme developed by Gizis (1997) which employs measures of the CaH and TiO bands in the 6300–7100 Å spectral region to form the indices CaH1, CaH2, CaH3, and TiO as defined in Reid et al. (1995). The locations in the three diagrams for the CaH indices versus the TiO index serve to separate the stars into three spectral metallicity classes designated MV for dwarfs with $[M/H] \approx 0.0$, sdM for the cool counterparts to the classical sdF–sdG subdwarfs with $[M/H] \approx -1.2 \pm 0.3$, and esdM for extreme subdwarfs with $[M/H] \approx -2.0 \pm 0.5$ (Gizis & Reid 1997). The numerical spectral subclass is then determined from calibrated relations with both the CaH2 and CaH3 indices. At the time that this classification scheme was established, there was only one star with subclass type later than sdM4.5 known – namely LHS377, which was assigned the type sdM7 “by

definition” (Gizis & Harvin 2006).

It has since become routine to consolidate the essential features of the Gizis classification scheme into a single diagram consisting of [CaH2 + CaH3] versus TiO5 (cf., Lépine et al. 2004), retaining the revised divisions between the three metallicity subclasses proposed by Burgasser & Kirkpatrick (2006). Further revision and extension of the Gizis system have been proposed by Lépine et al. (2007). A fourth subclass designated “usdM” indicating “ultrasubdwarfs” was added to the three-subclass scheme to recognize the relatively few M stars which apparently have metallicities as low as or perhaps below $[M/H] = -2.5$. A realignment of the subclass separators was put forward based on a new index, $\zeta_{\text{TiO}/\text{CaH}}$, which measures the calibrated TiO5 spectral index as a function of the [CaH2 + CaH3] index and is expressed as a ratio with the solar metallicity value. The separators are chosen so that they run parallel to the locii in the [CaH2 + CaH3, TiO5] plane for the observed components of wide common proper motion binaries with different spectral subtypes. A proposed list of subdwarf spectral classification standard stars were presented covering types K7.0 through M8.5 for each of the subclasses subdwarf, extreme subdwarf, and ultrasubdwarf. As further suggested by Burgasser et al. (2005), one really needs to simultaneously utilize spectral classification criteria from a wider range of wavelengths and low-resolution data covering the range 0.7–2.5 μm as a possible way to proceed in the future.

However, while the number of earlier type M subdwarfs recognized in the greater solar neighborhood has grown to several hundred due to these survey efforts, subdwarfs with types sdM6 and later remain relatively rare. Even as recently as this past year, the number of subdwarfs with types sdM7 or later numbered only around 15 (Burgasser et al. 2007; Lépine et al. 2007). The discovery of one of these few – LSR1425+7102, hereafter referred to as LSR1425+71 – was announced several years ago by Lépine et al. (2003b) and assigned a classification of sdM8.0 on the Gizis (1997) system, making it the coolest sdM star identified at that time. The similarity in overall continuum slope with LSR2000+3057 (M6.0V) over the 6000 – 9000 Å spectral region was noted. Employing the Baraffe et al. (1997; hereafter BCAH97) “NextGen” model atmospheres for a metal-poor $0.09M_{\odot}$ star with $[Fe/H] = -1.3$ to estimate the absolute magnitude, they derived a “conservative distance estimate of 65 ± 15 pc.” This distance, when combined with their measured proper motion of $0.635 \text{ arcsec yr}^{-1}$ in a position angle of 254.7 deg and their measured radial velocity of $-65 \pm 20 \text{ km s}^{-1}$, yielded space velocity components of $(U, V, W)^1 = (-65 \pm 22, -177 \pm 35, +64 \pm 27) \text{ km s}^{-1}$, consistent with halo membership. Note that LSR1425+71 is also adopted as the classification standard star for spectral type sdM8.0 by Lépine et al. (2007).

¹ Throughout this paper, U is measured radially outward toward the galactic anticenter.

Later in 2003, the same investigators announced the discovery of LSR1610–0040, hereafter referred to as LSR1610–00, and suggested that it might be an early-type sdL subdwarf (Lépine et al. 2003a; hereafter LRS03). At that time the only other sdL candidate was 2MASS 0532 + 8246 discovered by Burgasser et al. (2003) from spectroscopic follow-up on 2MASS photometric candidates. Lépine et al. (2003a) noted that while their optical spectrum of LSR1610–00 (coverage $\approx 6000 - 10,000 \text{ \AA}$; resolution $\approx 7 \text{ \AA}$) showed obvious similarities to their spectrum of LSR1425+71, LSR1610–00 possessed a distinctly steeper pseudocontinuum (implying a cooler temperature) and, more significantly, showed strong Rb I 7800, 7947 \AA lines which are more typically present in L-type dwarfs rather than M-dwarfs. With its weak TiO bands and totally absent VO bands LSR1610–00 did not fit anywhere in the known sequences of dwarf M or subdwarf M stars. Again using the BGAH97 models, they “conservatively” estimated the distance to LSR1610–00 to be $16 \pm 4 \text{ pc}$. Centroids of the Rb I lines together with those from the K I doublet (7665, 7699 \AA) yielded a heliocentric radial velocity of $-130 \pm 20 \text{ km s}^{-1}$. Using their measured proper motion of $1.46 \text{ arcsec yr}^{-1}$ in a position angle 212.0 deg yields galactic space velocity components of $(U,V,W)=(-117\pm 18, -108\pm 24, -10\pm 19) \text{ km s}^{-1}$, suggesting that LSR1610–00 is most likely a member of the old disk population.²

Combining new moderate resolution spectroscopy covering $0.8\text{--}4.1 \mu\text{m}$ with the $0.6\text{--}1.0 \mu\text{m}$ data from LRS03, Cushing & Vacca (2006; hereafter CV06) made a comprehensive study of the peculiarities and contradictions presented in the spectrum of LSR1610–00. Similar spectral data for three other sdM stars (LHS 3409, sdM4.5; LHS 1135, sdM6.5; LSR2036+5059, sdM7.5) and the M6.0V star GL406 were employed for comparison. GL406 is the well-studied high proper motion star Wolf 359 which is a primary MV spectral classification standard (Kirkpatrick et al. 1991) and a well established active flare star (CN Leo). Based on its (U,V,W) galactic kinematic components, GL406 is formally a member of the old disk population (Leggett 1992). However, Pavlenko et al. (2006) argue that its age is most likely younger than 0.4 Gyr – that is, younger than the Hyades cluster (age $\sim 0.6 \text{ Gyr}$) which is often taken as the upper age limit for the young disk population. CV06 concur with LRS03 that, in terms of spectral features, LSR1425+71 is a better match with LSR1610–00 than is GL406. On the other hand, in terms of overall relative spectral energy distribution (SED) over the entire wavelength range $0.6\text{--}4.1 \mu$, LSR1610–00 and GL406 are remarkably similar, despite the fact that some features in the $7640\text{--}8300 \text{ \AA}$ spectral region are notably dissimilar, especially the stronger TiO bandhead and the much weaker Rb I doublet in Gliese 406. Given all of the contradictory evidence summarized by CV06 (see Table 3),

²Note that the U, V, W values presented in Table 1 of LRS03 are incorrect, even for the input values these authors employ.

these authors conclude that LSR1610–00 is most likely a mildly metal-poor, mid-M dwarf but further call the star “schizophrenic” to acknowledge its several spectral peculiarities. In particular we note the abnormally strong Al I doublet at $1.313\ \mu\text{m}$ which suggests that aluminum is most likely overabundant compared with solar.

In a study concurrent with that of CV06, Reiners & Basri (2006; hereafter RB06) obtained high-resolution ($R \approx 31000$) spectra in several windows of the $0.7\text{--}1.0\ \mu\text{m}$ region for LSR1610–00, GL406, and 2MASS 1439+1929 (hereafter, 2M1439+19). The latter is a L1V star with an established trigonometrically determined luminosity (Dahn et al. 2002). Comparison of the strengths of TiO bands with heads at 7050, 8430, and $8870\ \text{\AA}$ do not preclude the possibility that LSR1610–00 might be slightly metal deficient. On the other hand, comparison of metal hydride bands (e.g., CaH at $6800\ \text{\AA}$ and FeH at $9900\ \text{\AA}$) indicate that LSR1610–00 can not be very much more metal-deficient than is GL406. As pointed out earlier by both LRS03 and CV06, the primary discrepancies arise for a few atomic lines. In particular, the Rb I lines at 7947 and $7800\ \text{\AA}$ agree much better with those in 2M1439+19, not only in strength but in shape. In contrast, the Cs I lines at 8520 and $8944\ \text{\AA}$ are much weaker in LSR1610–00 than in 2M1439+19, with the redder one being almost undetectable. Not only are the Cs I lines more similar to those in GL406, the one at $8520\ \text{\AA}$ is significantly stronger than in GL406. The strengths of the Ca II triplet components at 8498 and $8542\ \text{\AA}$ imply that LSR1610–00 must be at least as warm as GL406. Comparing the spectra of LSR1610–00 and 2M1439+19 with PHOENIX atmospheric model predictions (cf., Allard et al. 2001), RB06 found that the observed Rb I and Cs I lines *could* be simultaneously reproduced at a satisfactory level by a slightly metal-deficient model ($[\text{Fe}/\text{H}] \approx -1$) with $T_{\text{eff}} = 2800\ \text{K}$, which alters the pseudo-continuum level appropriately for LSR1610–00.³ Based on this result RB06 suggested a spectral type of sd?M6 would be appropriate. However, given the remaining spectral peculiarities not addressed by RB06, we prefer to adopt the spectral type designation of sd?M6pec for the present. Finally, RB06 measured a high-precision heliocentric radial velocity for LSR1610–00 of $-95 \pm 1\ \text{km s}^{-1}$ by cross-correlating its spectrum with that of GL406 in the spectral region around $8000\ \text{\AA}$. They discuss the discrepancy between their result and that of LRS03 ($-130 \pm 15\ \text{km s}^{-1}$) measured from much lower resolution spectroscopy and suggest that the LRS03 value might require a corrective offset of $+20\ \text{km s}^{-1}$.

Calibration of the extension to the Gizis subdwarf-M spectral classification system to

³Lépine et al. (2004) announced the discovery of LSR0822+1700 as a second subdwarf M star that showed both RbI and CsI lines. In this instance, the location in the [CaH2 + CaH3, TiO5] plane clearly indicates low metallicity. LSR0822+1700 has been designated as a usdM7.5 spectral classification standard star by Lépine et al. (2007). USNO initiated a parallax determination for this star in March 2008.

physical parameters such as total luminosities and effective temperatures, such as proposed by Lépine et al. (2007), will require reliable trigonometrically determined distances. A representative sample of such M-type subdwarfs is currently being observed at the Flagstaff Station. Both LSR1425+71 and LSR1610–00 were added to the USNO CCD trigonometric parallax program back in the spring of 2003 and reliable results are now available for these two stars. Since LSR1425+71 and LSR1610–00 have been discussed and compared with one another repeatedly in the literature, we present our results for both stars together here.

2. Observations

The new observations presented here include: 1) parallax astrometry for both LSR1425+71 and LSR1610–00; 2) BVI photometry for both stars; and 3) a new radial velocity measure for LSR1610–00. The parallax astrometry was carried out with the 1.55 m Strand Astrometric Reflector at the Flagstaff Station of the US Naval Observatory using the TEK2K CCD Camera. The observational procedures followed were those summarized previously in Dahn et al. (2002). The astrometrically flat wide-I filter was employed for both fields. Photometry on the Johnson–Cousins system was obtained in the BVI bandpasses for both fields using the USNO 1 m telescope and following standard procedures (i.e., standard stars from Landolt 1992 observed each night; small color terms determined and applied nightly). Differential color refraction corrections for astrometric observations taken slightly off the meridian were derived from the V–I colors of the parallax star and the reference stars employed, as described in Monet et al. (1992). The corrections from relative to absolute parallax were derived from photometric parallaxes of the individual reference stars using M_V versus V–I relations calibrated with stars with large trigonometric parallaxes. The new radial velocity measure of LSR1610–00 was obtained using the University of Arizona/Harvard–Smithsonian 6.5 m MMT reflector. Details regarding the results follow.

2.1. Astrometric and Photometric Results for LSR1425+71

A total of 73 acceptable observations of this field have been obtained since it was added to the active program in April 2003, providing a total epoch coverage of over 4 years. The absence of suitable reference stars close to the parallax star has necessitated the use of a fairly spread out frame which extends to about 3 arc minutes from the target star. However, since the exposure times for this field are typically 15–20 minutes (depending on seeing and transparency) good averaging over atmospheric fluctuations was achieved resulting in formal rms single observational errors for the reference stars of ± 2.14 mas and ± 2.25 mas in RA

and DEC, respectively.

The astrometric and photometric results are presented in Table 1. As we shall show in Section 3 below, our parallax and photometry confirm the dwarf status of LSR1425+71 in three color–absolute magnitude diagrams. Likewise, adopting the radial velocity of -65 ± 20 km s⁻¹ measured by Lepine et al. (2003b), the derived U, V, W galactic kinematic components are entirely consistent with a halo population star, but see Sec. 5 below.

2.2. Astrometric and Photometric Results for LSR1610–00

Astrometric observations of LSR1610–00 commenced in June 2003 and by early 2005 the residuals from the solution for parallax and proper motion clearly indicated that this object is an unresolved, astrometric binary. Observational coverage of the field was intensified at that time. To date, a total of 219 acceptable observations spanning an epoch range of over 4 years has been obtained on this field. Our results indicate that over two full periods of the astrometric orbit have now been covered, permitting solutions for the photocentric orbital elements as well as the parallax and proper motion for this binary system.

In carrying out the astrometric reductions for LSR1610–00 we have chosen to employ an iterative procedure wherein the standard algorithms were first solved for parallax and proper motion. The residuals from this solution were then solved for the motion of the center of light about the center of mass. This resulted in preliminary orbital elements for the photocenter. These elements were then used to “correct” the originally measured parallax star positions, after which the solution was rerun for parallax and proper motion. The residuals from this revised solution were then resubmitted to the binary star reduction algorithms to obtain refined orbital elements. This iterative process was repeated until convergence had been achieved. Only four iterations were required.

The results for LSR1610–00AB are summarized in Table 2 and the derived orbital parameters for the photocentric orbit are presented in Table 3. Figure 1 shows the the residuals in RA and DEC after both the parallax and proper motion of the system have been removed, and the Table 3 orbit fit to these data. In general, the derived orbital elements appear to be quite robust. The possible exception is the eccentricity, because observations at phases around periastron passage are still not as numerous as desirable. Upcoming observations during the March–October 2008 interval should resolve this situation since we predict that the photocenter will pass through eastern elongation during this window.

We also note that since the observer’s line of sight to the LSR1610–00AB system is only 6.8 ± 1.0 degrees out of the plane of the photocentric orbit, the question of possible eclipses is

raised. However, as we shall conclude in Section 4, the radii of the most probable components are small. No evidence of eclipses can be seen in our astrometric observations, but our time coverage during anticipated close passages is too spotty to provide any meaningful constraint.

Our confirmation that LSR1610–00 is indeed an unresolved binary system opens a new dimension for understanding the seemingly “schizophrenic spectrum” of LSR1610–00 described by CV06. However, as we shall discuss in Section 4, the published radial velocities available for this star in the literature – $-130 \pm 20 \text{ km s}^{-1}$ at Epoch = 2003.137 by LRS03 and $-95 \pm 1 \text{ km s}^{-1}$ at Epoch = 2005.167 by RB06 – present difficulties for interpreting our photocentric orbit. Hence, priority was given to obtaining a new, independent measure of the radial velocity at an orbital phase different from those of the earlier results.

2.3. A New Radial Velocity Measure for LSR1610–00AB

The radial velocity observation of LSR1610–00 was obtained on 2006 March 6 (U.T.) using the 6.5 m MMT and red channel spectrograph. Based on the astrometry for the apparent orbit available at that time we anticipated that the photocenter of the system would be near elongation during the spring of 2006. The 1200 g/mm grating blazed at 7700 Å was employed yielding a resolution of 2.1 Å with a one arc second slit width. The wavelength coverage used for the measurements was from about 7640 Å (omitting the edge of the spectrum in the atmospheric “A” band) to 8300 Å. The principal strong lines encompassed in this spectrum include the K I resonance doublet at 7665, 7699 Å, the Rb I doublet at 7800, 7947 Å, and the subordinate Na I 8183, 8194 Å doublet. GL406 was observed as a radial velocity standard for cross-correlation reductions.

The observations were generally obtained in pairs of 600 second and 300 second integrations for LSR1610–00 and GL406, respectively. Each pair was bracketed by observations of the helium-neon-argon arc lamp at the position of the object. Excellent wavelength fits were obtained after extractions of the two-dimensional images to obtain object apertures, using standard IRAF tasks for this purpose. Separate solutions for all arc / object pairings were always accurate to better than $\pm 0.1 \text{ Å}$, generally accurate to $\approx \pm 0.05 \text{ Å}$. Cross-correlations were carried out between each of the six LSR1610–00 observations and each of the eight observations of Wolf 359 using the IRAF task “fxcor”.

Difficulties with employing the cross-correlation approach were encountered due to the extreme fringing of the chip at these wavelengths, resulting in 50–100 Å “bumps” which could not be removed by the flatfields. Attempts at filtering the data in favor of the smaller spacings of the atomic lines did not alleviate these difficulties. Consequently, the cross-correlation

technique was abandoned and the radial velocity of LSR1610–00 was determined from line profile fittings to four individual lines – Rb I (7800, 7947 Å) and Na I (8183, 8194 Å) – for each of the six LSR1610–00 spectra. The actual wavelength values (in air) employed for these four lines (7800.268, 7947.603, 8183.256, and 8194.824 Å, respectively) were obtained from the current National Institute of Standards and Technology Atomic Spectra Database Web site (NIST 2008). Rejecting one of the six LSR1610–00 observations as an obvious outlier, the remaining five observations yielded a measured radial velocity of -135.7 km s^{-1} . Applying a calculated correction of $+27.6 \text{ km s}^{-1}$ to convert this to heliocentric, we obtain $V_{\text{rad}} = -108.1 \pm 1.6 \text{ km s}^{-1}$ at Epoch = 2006.179.

Even allowing for reasonable orbital variation, the LRS03 result is not compatible with the more recent measures determined from significantly higher resolution spectra. RB06 discussed the possible need for a roughly $+20 \text{ km s}^{-1}$ adjustment to the LRS03 value based on similar systematic effects noted by Burgasser et al. (2003) in the case of radial velocity measures for 2MASS 0532+8246. However, the large formal uncertainty attached to the LRS03 value alone renders this measure of little value in assessing the nature of the LSR1610–00AB binary system. Hence, we will disregard the LRS03 radial velocity measure from further consideration. Taking into account the orbital phases of the RB06 determination and our new observation (cf. Figure 1), we conclude that the systemic velocity of the LSR1610–00AB is approximately $-101 \pm 1 \text{ km s}^{-1}$ and that the velocity semi-amplitude for the photocenter of the binary is $\lesssim 7 \text{ km s}^{-1}$. With this systemic velocity and the parallax and proper motion, we calculate the U, V, W galactic kinematic components given in Table 2. They are indicative of a halo population star, but see Sec. 5 below.

3. Locations in Color–Magnitude Diagrams

With reliable trigonometrically determined distances now available for both LSR1425+71 and LSR1610–00AB, these stars can be placed in a variety of absolute magnitude versus color diagrams (CMDs) to assess these stars’ relationship to each other, and to field M-dwarfs and sdM stars in general. Evolutionary stellar models should provide additional guidance toward understanding the status of both stars and, in particular, for inferring what viable components might comprise the LSR1610–00AB system. Models for stars with masses corresponding to dwarf M and L spectral types have been developed by several groups over the past decade, most notably those by the Lyon collaboration (BCAH97; Baraffe et al. 1998, hereafter BCAH98; Chabrier et al. 2000), by the University of Arizona group (Burrows et al. 2001; Burrows et al. 2006), and most recently by the collaborators modeling the HST ACS (Advanced Camera for Surveys) photometric survey of Galactic globular clusters (Sarajedini

et al. 2007; Dotter et al. 2007). While differing in a variety of details, the gross properties of the results from these three efforts agree where they overlap in terms of mass and metallicity. Hence, we will restrict comparisons below primarily with the Lyon models whose results are directly accessible in terms of absolute magnitudes and colors.

In presenting the Lyon models, BCAH97 and BCAH98 gave particular attention to three such diagrams – M_V versus $V-I$, M_K versus $I-K$, and M_K versus $J-K$. These three CMDs are discussed in turn in the following subsections.

3.1. The M_V versus $V-I$ Diagram

The locations of LSR1425+71 and LSR1610–00AB in the observed M_V versus $V-I$ diagram are presented in Figure 2. Included for reference are a selection of field dwarfs and subdwarfs which possess both (a) published USNO trigonometric parallaxes, and (b) VI photometry determined at the Flagstaff Station. The parallax determinations can be found in Harrington et al. (1993; and earlier papers cited therein), Monet et al. (1992), Dahn et al. (2002), and Reid et al. (2003).

Where parallax determinations are also available from other observatories (mainly for brighter stars), the weighted mean parallaxes as derived by van Altena et al. (1995) were adopted. The photometry includes considerable unpublished VI measures carried out at the Flagstaff Station over many years. M-type dwarfs are plotted as filled circles and 5 early L-type dwarfs are included as filled triangles. Dwarf stars are included in Figure 2 only if the formal errors for the parallax and the V magnitude combine for a formal uncertainty in M_V of ± 0.15 mag or less. This restriction results in enough data points both to map out the primary main sequence and also to illustrate the real physical spread of stars in this region of the diagram, presumably due to small variations in metallicity (Bonfils et al. 2005) and due to unresolved binary pairs. Subdwarfs are represented by open circles in Figure 2 and those shown are restricted to stars with formal uncertainties in M_V of ± 0.45 mag or less. All stars are plotted with their formal errors in both coordinates displayed. Three late-type dwarfs either known to be binaries (2M0149+29 and 2M0746+20) or suspected of being binary (2M0345+25) are flagged with ‘d’ and ‘d?’, respectively. Also labeled in Fig.2 are GL406 (M6.0V) and LHS377 (sdM7), the lowest luminosity M-type subdwarf with a trigonometrically determined distance (Monet et al. 1992) known to date.

Three conclusions can be drawn from the star locations in Figure 2 alone. First, in terms of overall match in SEDs, the similarities between LSR1610–00AB and GL406 noted by CV06 for wavelengths longer than $0.6 \mu\text{m}$ must extend at least down through wavelengths

corresponding to the V bandpass – that is, at least to $0.5 \mu\text{m}$. Furthermore, the similarities here established are for *absolute* energy distributions, not merely *relative* ones. Second, the components comprising LSR1610–00AB can not include objects like either LSR1425+71 or LHS377 since both of these stars are significantly more luminous in M_V and bluer than the combined light from the astrometric binary system. Finally, it is unlikely that one can invoke a normal, early-type dL star as the B component of the LSR1610–00AB system in order to explain the strong Rb I 7800, 7947 Å lines seen in the Lépine et al. (2003a) optical spectrum. In the I-bandpass, even the earliest L dwarfs are approximately 2 magnitudes fainter than what would be required for an A component satisfying the location of the combined light in Fig. 2. Such a large magnitude difference would greatly reduce the visibility of the Rb I lines, most likely rendering them undetectable.

Models with solar (or near solar) metallicity continue to present problems, especially for wavelengths shortward of $\sim 1.0 \mu\text{m}$ where important molecular opacity sources are still not included or are incomplete. Some aspects of the current status of such models are illustrate in Figure 2 by the solid black line which represents the NextGen (BCAH98) isochrone for stars with masses $\geq 0.1 M_\odot$ for an evolved age of 0.5 Gyr and by the solid red line which represents the DUSTY (Chabrier et al. 2000) isochrone for stars with masses $\leq 0.1 M_\odot$, also for an evolved age of 0.5 Gyr. For $M_V < 19$ ($T_{\text{eff}} > 2800$ K) dust formation is unimportant implying that the offset between the NextGen and DUSTY models is primarily due to improved treatment of atmospheric opacity for TiO and, to a lesser extent, CaH (Allard et al. 2000). Still, the models remain too blue by 0.1–0.2 mag in the region of Figure 2 corresponding to LSR1610–00AB and GL406. While better agreement between the DUSTY models and the field dM stars is realized for a model evolutionary age of 0.1 Gyr (see Chabrier et.al 200, Fig. 4, and the dotted red line in the present Fig. 2.), such a young age (younger than the Pleiades cluster!) is certainly unrealistic for the mixture of young/old disk population field M-dwarfs in the solar neighborhood (Leggett 1992).

The blue lines in Figure 2 represent the BCAH97 isochrones for metal deficient stars with $[M/H] = -1.0, -1.5,$ and -2.0 and ages ≥ 5 Gyr. These models appeared to be in satisfactory agreement with both the HST observations of three globular clusters (M15, NGC6397, ω Cen) and field halo subdwarfs with trigonometrically determined distance. All of the aforementioned data seemed to be well represented by isochrones with metallicities $[M/H] \sim -1.3$ to -1.5 , corresponding to $[Fe/H] -1.6$ to -1.8 when allowance for oxygen enhancement over the evolutionary age of the Galaxy is taken into account. This agreement provided hope that the BCAH97 models might be reliable for detailed comparison with observations of metal-deficient stars where the importance of double-metal molecular bands (e.g., TiO, VO) are expected to be less important. However, at the time of the BCAH97 paper, the globular cluster observations extended only down to luminosities of $M_V \sim 12$

and the observed field subdwarfs only reached down to $M_V \sim 14.5$. Figure 2 shows that model predictions for $-2.0 \leq [M/H] \leq -1.0$ effectively converge for the range of interest for LSR1425+71 and LSR1610–00AB, that is for M_V between ~ 15.0 and ~ 17.0 . We note that both of the subdwarfs LSR1425+71 and LHS377 lie roughly 0.2 mag above the model locii (or alternately, about 0.1 mag redward of the models).

The less than satisfactory agreement between the observations of subdwarfs with types of early-M or later and current metal-deficient models in the M_V versus $V-I$ diagram is almost certainly a continuing problem with the models. The recent study of NGC6397 by Richer et al. (2007) demonstrated excellent agreement between models appropriate for the observed distance (≈ 2.6 kpc), metallicity ($[Fe/H] \approx -2.0$; $[\alpha/Fe] \approx +0.3$), and age (≈ 12 Gyr) of this cluster and the HST/ACS observed CMD for over 11 magnitudes of luminosity extending well into the giant branch, down through the cluster turnoff region, and for over 8 magnitudes of the cluster main-sequence. However, below a luminosity corresponding to $M_V \sim 13$ the same systematic discrepancy between the models and observations is seen for NGC6397 that we find in Figure 2. This undoubtedly reflects incompleteness in the model atmospheric opacities, especially at wavelengths shortward of $\sim 1.0 \mu\text{m}$. Consequently, we still must remain cautious when drawing detailed conclusions based on the locations of M-type dwarfs and subdwarfs in the M_V versus $V-I$ CMD.

3.2. The M_{K_s} versus $I-K_s$ Diagram

Less influence due to incomplete molecular opacity sources in the atmospheric model calculations is anticipated for infrared bandpasses. BCAAH98 discussed the M_K versus $I-K$ CMD, pointing out that it provided a “powerful diagnostic for metallicity.” Figure 3 shows locations of LSR1425+71, LSR1610–00AB, LHS377, and GL406 in the M_{K_s} versus $I-K_s$. Here we are using photometry extracted from the 2MASS point source catalog and retain the subscript “s” to distinguish the 2MASS short-K bandpass from the CIT bandpass. The filled and open circles are field dwarfs and subdwarfs, respectively, as in Figure 2. (Since the locii of dwarfs and subdwarfs merge in this CMD, and form a nearly vertical sequence, we only plot field stars for $M_{K_s} \geq 7.3$.) Also included in Figure 3 is 2MASS 0532+8246 (hereafter, 2M0532+82), the first L-type subdwarf discovered by Burgasser et al. (2003). A trigonometric parallax determined from ASTROCAM near-infrared observations carried out at the USNO Flagstaff Station places the star at a distance of 26.7 ± 1.2 pc and yields clear halo kinematic properties (Burgasser et al. 2008). Spectroscopically, 2M0532+82 is classified as sdL7 (Burgasser et al. 2007). (The adopted I magnitude used to plot 2M0532+82 in Figure 3 comes from Burgasser et al. 2008. Note that this star could not be included in

Figure 2 since a V magnitude is still unavailable.) The model locii included in Figure 3 are the same as those shown in Figure 2, except that we include here the BCAH97 $[M/H] = -1.3$ isochrone for ages ≥ 5 Gyr, in addition to those for $[M/H] = -1.0, -1.5,$ and -2.0 , since they are well separated in this CMD. The transformation relations derived by Carpenter (2001) have been applied to the BCAH97 tabulated values to convert them from the CTI photometric system to the 2MASS system employed here.

Some results to be noted from Figure 3 include the following. First, the field subdwarfs seem to be reasonably in accord with the BCAH97 metal-deficient isochrones for M_{K_s} below about 8.5. However, for $M_{K_s} < 8.0$ the isochrones run well to the blue side of the few observational points available. LSR1425+71 is located nearly on the model locus for $[M/H] = -1.3$, consistent with its being a later-type counterpart to the field sdF/sdG stars. It is interesting to note that LSR1425+71 is only about 0.3 mag less luminous in M_{K_s} than the two field subdwarfs LHS 1742a ($M_{K_s} = 9.74, I-K_s = 1.96$) and LHS 3061 ($M_{K_s} = 9.65, I-K_s = 1.99$). This contrasts to the relative locations of these three stars in Figure 2, where LHS 1742a is about 0.8 mag more luminous than LSR1425+71 in M_V and LHS 3061 is a full magnitude more luminous than LSR1425+71. Second, The relative locations of LSR1425+71 and LHS377 in Figure 3 indicate that LHS377 is significantly less metal deficient than LSR1425+71. Accepting the models at face value might lead to an estimate of $[M/H] \approx -0.8$ for LHS377. Third, the location of LSR1610–00AB in the midst of the disk field dwarfs again offers no clue to the nature of the individual components making up this binary. That is, it does not appear to be overluminous as would be the case if both components of the binary were contributing significant light to the photocenter. And finally, the sdL7 2M0532+82 lies alone in the lower part of Figure 4. Since the BCAH97 models include masses down to only $0.083 M_\odot$, no reliable inference concerning the metallicity of 2M0532+82 is possible from Figure 4. Burgasser et al. (2008) made a “best guess” estimate of $[M/H] = -1$, implying a mass of $0.0783 \pm 0.0013 M_\odot$ for this unique object.

As was the case in Figure 2, the DUSTY model isochrone for an age of 0.5 Gyr (solid red line) does a poor job in representing the field dwarfs. Likewise, the DUSTY model isochrone for an age of 0.1 Gyr (dotted red line), while in better agreement with the observational points, is still not fully satisfactory.

3.3. The M_{K_s} versus J– K_s Diagram

If the discrepancies noted in the previous two CMDs between observations of field M-dwarfs and solar metallicity model isochrones is primarily due to incompleteness in the atmospheric opacities for wavelengths blueward of $\sim 1.0 \mu\text{m}$, improved agreement might be

expected for the M_{K_s} versus $J-K_s$ CMD. Figure 4 shows the stars under consideration in that CMD where the field dwarfs and subdwarfs, as well as model isochrones included, are the same as in Figure 3. As before, the model data points have been converted from the CTI photometric system to the 2MASS system via the Carpenter (2001) transformations. While shape-wise the locii for both DUSTY model isochrones (red solid and dotted lines) better reflect the trend of the M-dwarf observations to branch off to redder $J-K_s$ below $M_{K_s} \approx 10.0$, the 0.5 Gyr isochrone (solid red line) fails to reproduce the field M-dwarf observations at all colors and luminosities plotted here. Even the 0.1 Gyr isochrone (dotted red line) fails to provide a satisfactory fit.

The field subdwarfs, including both LSR1425+71 and LHS377, seem to be well reproduced by the BCAH97 models in Figure 4. Again, accepting the fits at face value would imply metallicities of $[M/H] \approx -1.5 \pm 0.3$ and $[M/H] \approx -1.0 \pm 0.2$ for LSR1425+71 and LHS377, respectively. The location of LSR1610–00AB amongst the field M-dwarfs in a region of the diagram where the trend of the observational data points is nearly vertical prevents us from inferring much of interest about possible components for the system. We can note, however, that there is nothing to suggest that LSR1610–00AB is a subdwarf.

In summary then, the CMDs discussed here all seem to support LSR1425+71 being a later-type counterpart to the classical sdF/sdG field subdwarfs while LSR1610–00AB exhibits no subdwarf characteristics. Both the field M-dwarfs and the field M-subdwarfs remain inadequately reproduced by current models in the M_V versus $V-I$ CMD. The field M-subdwarfs seem to be reproduced satisfactorily in both the M_{K_s} versus $I-K_s$ and the M_{K_s} versus $J-K_s$ CMDs. The solar metallicity and near-solar metallicity models fail to adequately represent the field star M-dwarf data points in all three CMDs. Hence, no substantive inferences can be drawn about the components comprising the LSR1610–00AB binary from these diagrams.

3.4. The B–V versus V–I Diagram

The similarities in SEDs between GL406 and LSR1610–00AB noted in the above three CMDs do not, apparently, extend to wavelengths as short as the B bandpass. Figure 5 shows the location of the stars in the B–V versus V–I color–color diagram. Unfortunately, there are only a limited number of late-type parallax dwarfs and subdwarfs with measured B magnitudes, since they are generally very faint at shorter wavelengths. The filled and open circles in Figure 5 are the dwarfs and subdwarfs, respectively, shown in Figure 2 where B–V photometry is available. The open triangles are stars spectroscopically classified as subdwarfs with Flagstaff Station photometry but lacking suitably precise parallax distance determina-

tions at this time. As is well recognized (e.g., Dahn et al. 1995; Fig. 3), subdwarfs usually lie above the dwarfs in B–V versus V–I and by amounts which appear to correlate with metal deficiency. Figure 5 indicates that the blue flux from the atmospheres of LSR1610–00AB is highly suppressed when compared with GL406. Lacking spectroscopic coverage over the blue region at this time, we can only speculate about possible causes (see Sec. 6 below).

4. Inferring Plausible Components for the LSR1610–00AB System

The observed orbit given in Table 3 is that of the photocenter (the combined light) of the two components. The photocenter motion is identical to the motion of the primary A component if the secondary star contributes negligible light in the observing (*I*) bandpass. Note that the A and B components cannot be identical – that is, can not have the same masses and the same luminosities (at least not in the *I* bandpass). In such a system the center of light would track the center of mass exactly and there would be no astrometric perturbation. The general equation connecting the observed semi-major axis of the photocentric orbit, α , with the elements of the true orbit is

$$\alpha = a * (M_2 / (M_1 + M_2) - \beta) = a_1 * (1 - \beta * (M_1 + M_2) / M_2)$$

where a is the semi-major axis of the relative orbit of the two components (in AU), a_1 is the semi-major axis of the primary star (in AU), M_1 and M_2 are the masses of the primary and secondary components, respectively (in M_\odot), and

$$\beta = l_2 / (l_1 + l_2)$$

is the relative luminosity of the secondary star compared with the luminosity of the combined light (van de Kamp 1967). If the secondary star makes a negligible contribution to the combined light, then $\beta = 0$ and $a_1 = \alpha$; if it contributes significantly to the combined light, then $a_1 > \alpha$. As for any binary system, the masses must satisfy the general harmonic relation

$$a_1^3 / P^2 = M_2^3 / (M_1 + M_2)^2.$$

where P is the period in sidereal years.

Lacking direct observational information about the relative brightnesses of the individual A and B components at all wavelengths (and especially at *I* bandpass where the perturbation was observed), we can derive constraints about possible and impossible components from the observed orbit, the observed radial velocities, the CMDs, and our current knowledge regarding the mass–luminosity relationships (MLRs) for low-mass stars. An additional potential constraint is the failure to detect a companion in Keck II laser guide star adaptive optic

observations (Siegler et al. 2007). However, this null observation turns out to be of limited value because the observing epoch 2006.460 was at an orbital phase (Figure 1) where the photocenter was displaced from the barycenter by only 2 mas, implying a separation of the pair of only 5 mas, well below their sensitivity limits.

In fact, great progress has been achieved in the last few years in measuring dynamical masses for M dwarfs, both from ground based observations employing various combinations of precision radial velocities, adaptive optics imaging, and near infrared long baseline interferometry (Ségransan et al. 2000; Delfosse et al. 2000; Siegler et al. 2005; Siegler et al. 2007) and from space employing HST-FGS (Benedict et al. 2001; Henry 2004). As a result, there are now over two dozen M dwarfs with accurately determined masses (Ségransan et al. 2000; Ségransan et al. 2003). However, only one star, GJ1245C (= G208-44B = LHS3494B) with a dynamically measured mass of $0.074 \pm 0.005 M_{\odot}$ (Henry et al. 1999; Henry 2004), currently anchors the region $\lesssim 0.10 M_{\odot}$. Two additional binaries – GL569Bab, M8.5V+M9V, (Lane et al. 2001) and 2MASSJ0746425+2000321AB, L0V+L1.5V, (Bouy et al. 2004) – have astrometrically determined orbits and resulting total mass determinations which indicate individual components with masses $\lesssim 0.10 M_{\odot}$. Conversion to actual individual masses for both systems is, unfortunately, still model dependent at this stage. Hopefully, precision radial velocity measures will soon resolve the remaining ambiguities. We also acknowledge in passing that many new binaries with low-mass components and estimated periods as short as a few years have been identified recently (e.g., Forveille et al. 2005; Siegler et al. 2005; Siegler et al. 2007) and reliable dynamical mass determinations for a number of objects with masses $\lesssim 0.10 M_{\odot}$ should be forthcoming in just a few years.

We consider first the possibility that the secondary contributes virtually no light to the observed combined light in the I bandpass, here taken to mean $I_B - I_A \gtrsim 6.5$ mag so that $I_A - I_{A+B} \lesssim 0.01$ mag. Since all three CMDs presented in Section 2 above suggests that the A component lies very close to the dwarf main sequence, we estimate the mass for it from currently available empirical MLRs. As discussed by Delfosse et al. (2000), the current MLRs for near-infrared (JHK) bandpasses all show small observational dispersion and agree well with the predictions of the BCAH98 models whereas the M_V versus mass MLR shows considerably more scatter and increasing deviations from the models for masses $\lesssim 0.4 M_{\odot}$. For our initial estimate of the mass for LSR1610–00A we employ the Delfosse et al. (2000) polynomials fits to existing observations for $\log[M/M_{\odot}]$ versus M_V , M_J , M_H , and M_K . These relations yield a mean value of $0.095 M_{\odot}$ with a range of 0.098 – $0.090 M_{\odot}$.

The first three lines of Table 4 gives the solutions for the mass of the B component, assuming a possible range of masses for the A component as discussed above, and assuming that $\beta(I) = 0$. These solutions all require the companion object to have a mass near 0.06

M_{\odot} . Therefore it would certainly be a brown dwarf. It likely would have a spectral type of late-T or later, a temperature below 800 K, and a luminosity below $10^{-5.5} L_{\odot}$, although these quantities depend on the uncertain age and metallicity of the companion. These three solutions are self-consistent, in that the low mass required for the B component (near $0.06 M_{\odot}$) implies that it will not contribute significant light both in the I bandpass astrometric images and in the K bandpass spectrophotometric data.

Also included for each solution in Table 4 are the predicted radial velocity semi-amplitudes for the both the primary, K_1 , and for the secondary, K_2 , stars. Specifically, for the primary star we have, in km s^{-1} ,

$$K_1 = a_1 * \sin(i) / [0.0336 * P * \sqrt{(1 - e^2)}]$$

when a_1 is in AU and P is in sidereal years. The predicted radial velocity curve for the $\beta = 0$ solutions combined with our astrometric orbital elements is shown in Figure 6, along with the radial velocity observations from RB06 and this paper (see Section 2.3 above). Given the formal error estimates for the observations, the results seem to be self-consistent. While better definition of the observed radial velocity curve is certainly doable, it will require significant effort on a Keck class telescope.

Solutions were then carried out with $\beta(I) = 0.05$ and 0.10 , corresponding to a pair where $I_B - I_A \approx 3.2$ mag and 2.4 mag, respectively. These solutions require the B component to have a higher mass in the range 0.07 - $0.08 M_{\odot}$ in order to compensate for the increased semi-major axis of the relative orbit necessary to maintain the observed semi-major axis of the photocentric orbit. Then it would be near the star/brown dwarf boundary and could be either. The absolute magnitudes given in Table 4 for $\beta = 0.05$ and 0.10 are similar to those for 2M0532+82 (Burgasser et al. 2008), and our required mass for LSR1610–00B is consistent with the mass (0.074 - $0.082 M_{\odot}$) that Burgasser et al. estimated for 2M0532+82. One possible concern is that objects like 2M0532+82 have $I - J$ colors redder than LSR1610–00A, leading to the companion contributing more light at J (and probably at H and K , depending on its $J - K$ color). As discussed above, evidence for a composite infrared spectrum is not compelling. With present available data, however, these solutions cannot be ruled out.

Finally, solutions were attempted for a selection of $\beta(I)$ greater than 0.10 . The $\beta(I) = 0.15$ case corresponds to a pair where $I_B - I_A \approx 1.9$ mag. Solutions with $\beta > 0.10$ appear to be incompatible with the observed parallax and absolute magnitudes; as β is increased, the semi-major axis of the primary star becomes larger, the masses of both components must become larger to keep the orbit bound, and the high masses become inconsistent with any reasonable mass-luminosity relation and the observed absolute magnitudes. Therefore, we believe these possibilities are excluded.

For all the acceptable solutions given in Table 4, the sum of the semi-major axes of the two stars is 0.7–0.8 AU. Allowing for the observed eccentricity of the orbits, the separation between the two stars is 0.4–0.8 AU. This separation is sufficiently large that mass transfer cannot be occurring now and would not have occurred in the past unless through a phase of common envelope evolution.

5. Galactic Orbits for LSR1425+71 and LSR1610–00

The distances determined in this paper for LSR1425+71 and LSR1610–00, together with radial velocities, allow calculation of their space velocities and orbits through the galaxy. As mentioned in Sec. 2, the large negative V velocity for both stars is strongly indicative of a halo origin for both. To calculate their orbits, we modeled the orbits in three potentials, two extreme cases (a Keplerian point mass, and a Pseudo-isothermal sphere), and a quasi-realistic model (that of Dauphole and Colin 1995, which is made up of three Miyamoto-Nagai components, representing the bulge, disk and halo). The orbits were integrated using a Bulirsh-Stoer integrator. Following Kerr & Lynden-Bell (1986), the solar radius was presumed to be 8.5 kpc, and the circular velocity of the LSR $\Theta_0 = 220.0 \text{ km s}^{-1}$. The solar motion with respect to the LSR $(U, V, W) = (-10.0, 5.2, 7.2) \text{ km s}^{-1}$, where U points radially outward (Dehnen & Binney 1998). Energy was conserved at better than one part in 10^9 over the integrations. Integrations were run backwards in time for up to 3×10^9 years, in steps of 10^5 years. Figures 7 and 8 show the orbits in the Dauphole & Colin (1995) potential for the past 5×10^8 years.

For both stars, in all cases, the orbits are quite eccentric ($e > 0.6$, and typically closer to $e \sim 0.9$), highly inclined with respect to the galactic plane ($60 \lesssim i \lesssim 84 \text{ deg}$), have periods of roughly 100 Myr, and apo-galactica near the solar orbital radius. In both cases, the orbits are largely radial and variably vertical, with only a very modest amount of rotational motion in the $x - y$ plane.

For LSR 1610–00, the peri-galacticon distance ranges from 140 pc in the Dauphole & Colin model up to 1,460 pc for a simple pseudo-isothermal halo model (with a nice broad core). For LSR 1425+71, the peri-galacticon passage radii are 300 pc and 2030 pc, respectively. The total space velocities at peri-galacticon passages for the Dauphole & Colin model are 650 and 610 km s^{-1} for LSR1610–00 and LSR1425+71, respectively. Given how close both stars come to the galactic center, it is quite likely that both have undergone significant scattering within the last few orbital periods. Given the very small peri-galacticon distances (particularly for LSR1610–00), we felt it useful to assess the impact of the massive black hole at the Galactic center on the stellar orbits. We added a point mass component, of

$3.7 \times 10^6 M_{\odot}$ to the Dauphole & Colin model. Qualitatively, the results were the same. The highly inclined and eccentric nature of the orbits as seen now would argue that they are not originally disk stars, as the change in angular momentum would be quite substantial. Also, the fact that the orbital apo-galactica are near the solar radius would argue that they are not recent products of the far outer halo.

6. Further Discussion

Previously, both CV06 and RB06 have used extensive spectroscopic data to conclude that LSR1610–00 appears peculiar (even “schizophrenic”), but it is most likely to be mildly metal-poor with some elements (particularly enhanced aluminum) indicating an unusual composition. The absolute magnitudes and colors found in this paper support the idea that it is near solar metallicity, although the uniquely red B–V color may be another indicator of unusual composition. However, the revised distance in this paper and the space velocity and galactic orbit shown in Sec. 5 are paradoxical: the space velocity and orbit are not at all disk-like, and would normally indicate (although do not require) a lower metallicity than mildly metal-poor. The finding in this paper of a binary companion with a separation of less than 1 AU is a new surprise. Using Occam’s razor as a guiding principle, we might hope to relate the peculiar abundances to some interaction or mass transfer between the two binary components.

The enhancement of aluminum found by CV06 is probably an important clue. Halo red giants and more massive AGB stars may produce aluminum enhancements due to mixing burning products of the hydrogen shell to the surface. The aluminum is produced at the expense of oxygen (Kraft 1994). Hence, one possible scenario that might be considered is that LSR1610–00B, the astrometric companion to LSR1610–00A, is a white dwarf. During the RGB or AGB phase of the evolving white dwarf progenitor, an excess of aluminum was produced and mixed to the surface. With a 1.7 year period, depending on the stellar mass, the red giant might be big enough to transfer Al-enriched material to the small dwarf companion. This would result in the enhancement observed today.

It appears, however, that this scenario has fatal flaws and must be discarded. The fundamental difficulty is the low mass of both components required by the binary possibilities in Table 4. White dwarf masses below $0.2 M_{\odot}$ have been found as companions to millisecond pulsars (van Kerkwijk et al. 1996) and in the Sloan Digital Sky Survey (Eisenstein et al. 2006), although these are rare. What appears to be required to form a white dwarf of extremely low mass is that the companion has a separation such that Roche lobe overflow occurs when the primary star is trying to leave the main sequence with only a small helium

core. If this happens, the star does not become much bigger than its main sequence size before its evolution and growth of the core mass are truncated. As such, the 1.7 year period and the separation of the two stars of 0.4-0.8 AU are too long and too large for this to have occurred.

A second problem is that, even with a maximum cooling age on the order of that of the halo (~ 12 Gyr), most low-mass white dwarfs will still have a luminosity such that they will be visible in the spectrophotometry of LSR1610–00. The most stringent constraint is the observed $M_B = 22.4$ and $B-V = 3.3$, requiring $M_B > 25$ for a possible white dwarf companion. For example, white dwarf models from Bergeron et al. (1995) with hydrogen atmospheres and $M = 0.15 M_\odot$ reach $M_B = 19.1$ at a cooling age of 12 Gyr. It may be possible that a low-mass white dwarf with a helium atmosphere would cool quickly enough that it could still be present and not detected. Otherwise, the companion to LSR1610–00A must be an unevolved, lower-mass star or substellar brown dwarf. Therefore, the B component to LSR1610–00A appears not to be the source of abundance anomalies in LSR1610–00A.

Nevertheless, peculiar abundances do point toward the accretion of mass onto LSR1610–00. Most notable is the enhancement of Al found by CV06, a result suggesting accretion from a massive AGB star that has undergone hot-bottom-burning. Some stars in globular clusters (both giants and subgiants) have enhanced Al and Na, and depleted O, indicative of external pollution by AGB stars (e.g., Sneden et al. 2004). The mechanism for Al and Na production is believed to be proton capture by Mg and Ne nuclei at high temperatures at the base of the hydrogen-burning shell. The most extreme abundance anomalies of this type are seen in the extreme metal-poor star HE1327-2326 (Frebel et al. 2005) where C, N, Na, Mg, and Al are seen to be strongly enhanced compared to Fe, and Ca and Ti are mildly enhanced. We speculate that accretion of $< 0.05 M_\odot$ of material with such strong enhancements onto LSR1610–00, which initially might have been about $0.05 M_\odot$ and $[\text{Fe}/\text{H}] \sim -2$, followed by complete mixing in the fully convective star, can lead to the star we see now. The accretion enhances all elements, making LSR1610–00 mildly metal-poor, it enhances C and the C/O ratio, almost (but not quite) turning LSR1610–00 into a carbon star and leaving most oxygen tied up in CO, it enhances Ti, but leaves TiO slightly depleted, and it greatly enhances Al. The B bandpass includes several bands of AlH, as well as MgH, SiH, and CaI: these bands are likely to have enhanced strength in LSR1610–00 compared to most dM6 and sdM stars because of a combination of being mildly metal-poor (strengthening the hydrides and atomic lines) and abundance anomalies. We speculate that these (not yet observed) features are the cause of the unique red $B-V$ color.

The AGB star proposed to be the source of mass accretion probably would have been a more distant companion in a triple system. It would now be a cool white dwarf, and must

have separated from the present LSR1610–00 binary when it lost most of its mass. (If it were still bound with LSR1610–00, it would now be detectable as a companion, unless it was initially massive enough to become a neutron star.) Alternatively, LSR1610–00 and the AGB star originally could have been part of a globular cluster when the accretion occurred, with LSR1610–00 later being lost from the cluster or the cluster dissipating entirely.

Acknowledgments... The authors would like to express their sincere appreciation to Elizabeth “Betsy” Green for her advice and assistance in carrying out the reductions of the MMT radial velocity observations.

REFERENCES

- Allard, F., Hauschildt, P.H., Alexander, D.R., Tamanai, A., & Schweitzer, A. 2001, *ApJ*, 556, 357
- Allard, F., Hauschildt, P.H., & Schwenke, D. 2000, *ApJ*, 540, 1005
- Baraffe, I., Chabrier, G., Allard, F., & Hauschildt, P.H. 1997, *A&A*, 327, 1054 (BCAH97)
- Baraffe, I., Chabrier, G., Allard, F., & Hauschildt, P.H. 1998, *A&A*, 337, 403 (BCAH98)
- Benedict, G.F., et al. 2001, *AJ*, 121, 1607
- Bergeron, P., Wesemael, F., & Beauchamp, A. 1995, *PASP*, 107, 1047
- Bonfils, X., Delfosse, X., Udry, S., Santos, N.C., Forveille, T., & Ségransan, D. 2005, *A&A*, 442, 635
- Bouy, H., et al. 2004, *A&A*, 423, 341
- Burgasser, A.J. & Kirkpatrick, J.D. 2006, *ApJ*, 645, 1485
- Burgasser, A.J., Kirkpatrick, J.D., & Lépine, S. 2005, 13th Cambridge Workshop of Cool Stars, Stellar Systems, and the Sun (ESA-SP-560), ed. F. Favata, G.A.J. Hussain, & B. Battrick (Noordwijk: ESA), p. 237
- Burgasser, A.J., et al. 2003, *ApJ*, 592, 1186
- Burgasser, A.J., Cruz, K.L., & Kirkpatrick, J.D. 2007, *ApJ*, 657, 494
- Burgasser, A.J., Vrba, F.J., Lépine, S., Munn, J.A., Luginbuhl, C.B., Henden, A.A., Guetter, H.H., & Canzian, B.C. 2008, *ApJ*, 672, 1159
- Burrows, A., Hubbard, W.B, Lunine, J.I., & Liebert, J. 2001, *Rev. Mod. Phys.*, 73, 719
- Burrows, A., Sudarsky, D., & Hubeny, I. 2006, *ApJ*, 640, 1063
- Carpenter, J.M. 2001, *AJ*, 121, 2851
- Chabrier, G., Baraffe, I., Allard, F. & Hauschildt, P. 2000, *ApJ*, 542, 464
- Cushing, M.C. & Vacca, W.D. 2006 *AJ*, 131, 1797 (CV06)
- Dahn, C.C., Liebert, J., Harris, H.C., and Guetter, H.H. 1995, in *The Bottom of the Main Sequence – and Beyond*, ed. C.G. Tinney (Berlin: Springer-Verlag), 239

- Dahn, C.C., et al. 2002, *AJ*, 124, 1170
- Dauphole, B. & Colin, J. 1995, *A&A*, 300, 117
- Dehnen, W. & Binney, J. 1998, *MNRAS*, 298, 387
- Delfosse, X., Forveille, T., Ségransan, D., Beuzit, J.-L., Udry, S., Perrier, C., & Mayor, M. 2000, *A&A*, 364, 217
- Dotter, A., Chaboyer, B., Jevremović, D., Baron, E., Ferguson, J.W., Sarajedini, A., & Anderson, J. 2007, *AJ*, 134, 376
- Eisenstein, D.J., et al. 2006, *ApJS*, 167, 40
- Forveille, T., et al. 2005, *A&A*, 435, L5
- Frebel, A., et al. 2005, *Nature*, 434, 871
- Gizis, J.E. 1997, *AJ*, 113, 806
- Gizis, J.E. & Harvin, J. 2006, *AJ*, 132, 2372
- Gizis, J.E. & Reid, I.N. 1997, *PASP*, 109, 1233
- Harrington, R.S., et al. 1993, *AJ*, 105, 1571
- Henry, T.J. 2004, in *ASP Conf. Ser. 318, Spectroscopically and Spatially Resolving the Components of Close Binary Stars*, ed. R.W. Hilditch, H. Hensberge & K. Pavlovski (San Francisco: ASP), 159
- Henry, T.J., Franz, O.G., Wasserman, L.H., Benedict, G.F., Shelus, P.J., Ianna, P.A., Kirkpatrick, J.D., & McCarthy, D.W., Jr. 1999, *ApJ*, 512, 864
- Kerr, F. & Lynden-Bell, D. 1986, *MNRAS*, 221, 1023
- Kirkpatrick, J.D., Henry, T.J., & McCarthy, D.W., Jr. 1991, *ApJS*, 77, 417
- Kraft, R.P. 1994 *PASP*, 106, 553
- Landolt, A.U. 1992, *AJ*, 104, 340
- Lane, B.F., Zapatero Osorio, M.R., Britton, M.C., Martín, E.L., & Kulkarni, S.R. 2001, *ApJ*, 560, 390
- Leggett, S.K. 1992, *ApJS*, 82, 351

- Lépine, S., Rich, R.M., & Shara, M.M. 2003a, *ApJ*, 591, L49 (LRS03)
- Lépine, S., Rich, R.M., & Shara, M.M. 2007, *ApJ*, 669, 1235
- Lépine, S., Shara, M.M., & Rich, R.M. 2003b, *ApJ*, 585, L69
- Lépine, S., Shara, M.M., & Rich, R.M. 2004, *ApJ*, 602, L125
- Monet, D.G., Dahn, C.C., Vrba, F.J., Harris, H.C., Pier, J.R., Luginbuhl, C.B., & Ables, H.D. 1992, *AJ*, 103, 638
- NIST Web Site 2008, <http://physics.nist.gov/PhysRefData/ASD/index/html>
- Pavlenko, Ya.V., Jones, H.R.A., Lyubchik, Yu., Tennyson, J., & Pinfield, D.J. 2006, *A&A*, 447, 709
- Reid, I.N., Hawley, S.L., & Gizis, J.E. 1995, *AJ*, 110, 1838
- Reid, I.N., et al. 2003, *AJ*, 125, 354
- Reiners, A. & Basri, G. 2006, *AJ*, 131, 1806 (RB06)
- Richer, H.B., et al. 2007, preprint (astro-ph/0708.4030)
- Sarajedini, A. et al. 2007, *AJ*, 133, 1658
- Ségransan, D., Delfosse, X., Forveille, T., Beuzit, J.-L., Udry, S., Perrier, C., & Mayor, M. 2000, *A&A*, 364, 665
- Ségransan, D., Delfosse, X., Forveille, T., Beuzit, J.-L., Perrier, C., Udry, S., & Mayor, M. 2003, in *IAU Symp. 211, Brown Dwarfs*, ed. E.L. Martín (San Francisco: ASP), 413
- Siegler, N., Close, L.M., Cruz, K.L., Martín, E.L., & Reid, I.N. 2005, *ApJ*, 621, 1023
- Siegler, N., Close, L.M., Burgasser, A.J., Cruz, K.L., Marois, C., Macintosh, B., & Barman, T. 2007, *AJ*, 133, 2320
- Snedden, C., Ivans, I.I., & Fulbright, J.P. 2004, in *Origin and Evolution of the Elements*, ed. A. McWilliam & M. Rauch (Cambridge: Cambridge Univ. Press), 170
- van Altena, W.F., Lee, J.T., & Hoffleit, E.D. 1995, *The General Catalogue of Trigonometric Stellar Parallaxes* (4th ed.; New Haven: Yale Univ. Obs.)
- van de Kamp, P. 1967, in *Principles of Astrometry* (San Francisco: Freeman), 142

van Kerkwijk, M.H., Bergeron, P., & Kulkarni, S.R. 1996, ApJ, 467, L89

Table 1. Astrometric and Photometric Results for LSR1425+71

Result	Value
Epoch Range (yr)	4.95
No. Frames	85
No. Nights	81
No. Ref. Stars	16
Rel. Parallax (mas)	12.27 ± 0.45
Rel. Proper Motion (mas yr ⁻¹)	625.8 ± 0.2
P.A. of Proper Motion (degrees)	255.2 ± 0.1
Correction to Abs. Parallax (mas)	1.10 ± 0.25
Abs. Parallax (mas)	13.37 ± 0.51
V (n=4)	19.62 ± 0.02
B–V (n=2)	2.06 ± 0.05
V–I (n=4)	3.26 ± 0.02
M _V	15.25 ± 0.09
J ¹	14.83 ± 0.04
H ¹	14.43 ± 0.06
K _s ¹	14.34 ± 0.10
V _{rad} (km s ⁻¹) ²	-65 ± 20
U (km s ⁻¹)	84 ± 6
V (km s ⁻¹)	-202 ± 13
W (km s ⁻¹)	66 ± 14

¹From 2MASS All-Sky Point Source Catalog

²From Lépine et al. 2003b, Table 1

Table 2. Astrometric and Photometric Results for LSR1610–00

Result	Value
Epoch Range (yr)	4.27
No. Frames	219
No. Nights	139
No. Ref. Stars	15
Rel. Parallax (mas) ¹	30.74 ± 0.52
Rel. Parallax (mas) ²	30.02 ± 0.21
Rel. Proper Motion (mas yr ⁻¹) ¹	1447.2 ± 0.3
Rel. Proper Motion (mas yr ⁻¹) ²	1446.5 ± 0.2
P.A. of Proper Motion (degrees) ¹	213.4 ± 0.1
P.A. of Proper Motion (degrees) ²	213.3 ± 0.1
Correction to Abs. Parallax (mas)	1.00 ± 0.15
Abs. Parallax (mas) ²	31.02 ± 0.26
V (n=4)	19.10 ± 0.02
B–V (n=2)	3.26 ± 0.14
V–I (n=4)	4.05 ± 0.02
M _V (A+B)	16.56 ± 0.03
J ³	12.91 ± 0.02
H ³	12.32 ± 0.02
K _s ³	12.02 ± 0.03
V _{rad} (km s ⁻¹) ⁴	-101.0 ± 1.0
U (km s ⁻¹)	36 ± 2
V (km s ⁻¹)	-232 ± 2
W (km s ⁻¹)	-61 ± 2

¹Before removal of the astrometric perturbation

²After removal of the astrometric perturbation

³From 2MASS All-Sky Point Source Catalog

⁴Adopted systemic radial velocity (see Sec. 4)

Table 3. Photocentric Orbital Elements for LSR1610–00AB

Parameter	Value
Period (yr)	1.662 ± 0.012
α (mas) ¹	8.91 ± 0.31
α (AU) ¹	0.276 ± 0.010
i (deg)	83.2 ± 1.0
e	0.444 ± 0.017
ω (deg)	151.4 ± 4.6
Ω (deg)	102.8 ± 1.8
T ₀	2005.854 ± 0.020
RMS _{RA} (mas)	2.2
RMS _{Dec} (mas)	3.3

¹Semi-major axis of the photocentric orbit.

Table 4. Viable LSR1610–00AB Component Properties

β	Primary Star			M_I	M_K	Secondary Star			M_I	M_K
	M_1 (M_\odot)	a_1 (AU)	K_1 (km s^{-1})			M_2 (M_\odot)	a_2 (AU)	K_2 (km s^{-1})		
0.00	0.090	0.287	5.7	12.5	9.5	0.057	0.453	9.0	>18.	>15.
0.00	0.095	0.287	5.7	12.5	9.5	0.059	0.462	9.2	>18.	>15.
0.00	0.100	0.287	5.7	12.5	9.5	0.061	0.472	9.4	>18.	>15.
0.05	0.095	0.325	6.5	12.5	9.5	0.070	0.441	8.8	15.7	12.7
0.10	0.095	0.366	7.3	12.5	9.5	0.082	0.424	8.5	14.9	11.9

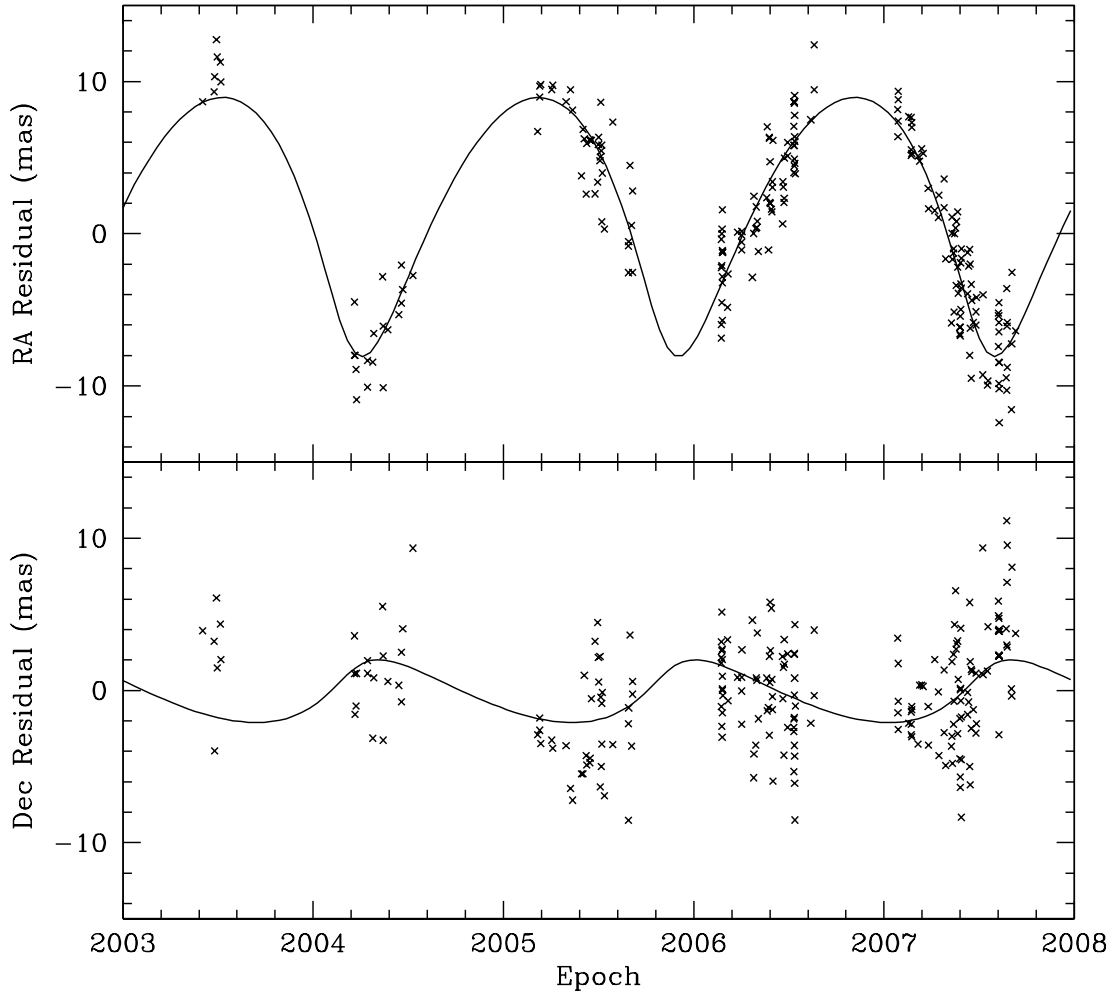


Fig. 1.— The positions in Right Ascension and Declination for the LSR1610–00AB photocenter after removing the parallactic and proper motions. The curves show the orbital motion fit to these residuals and represented by the orbital elements given in Table 3.

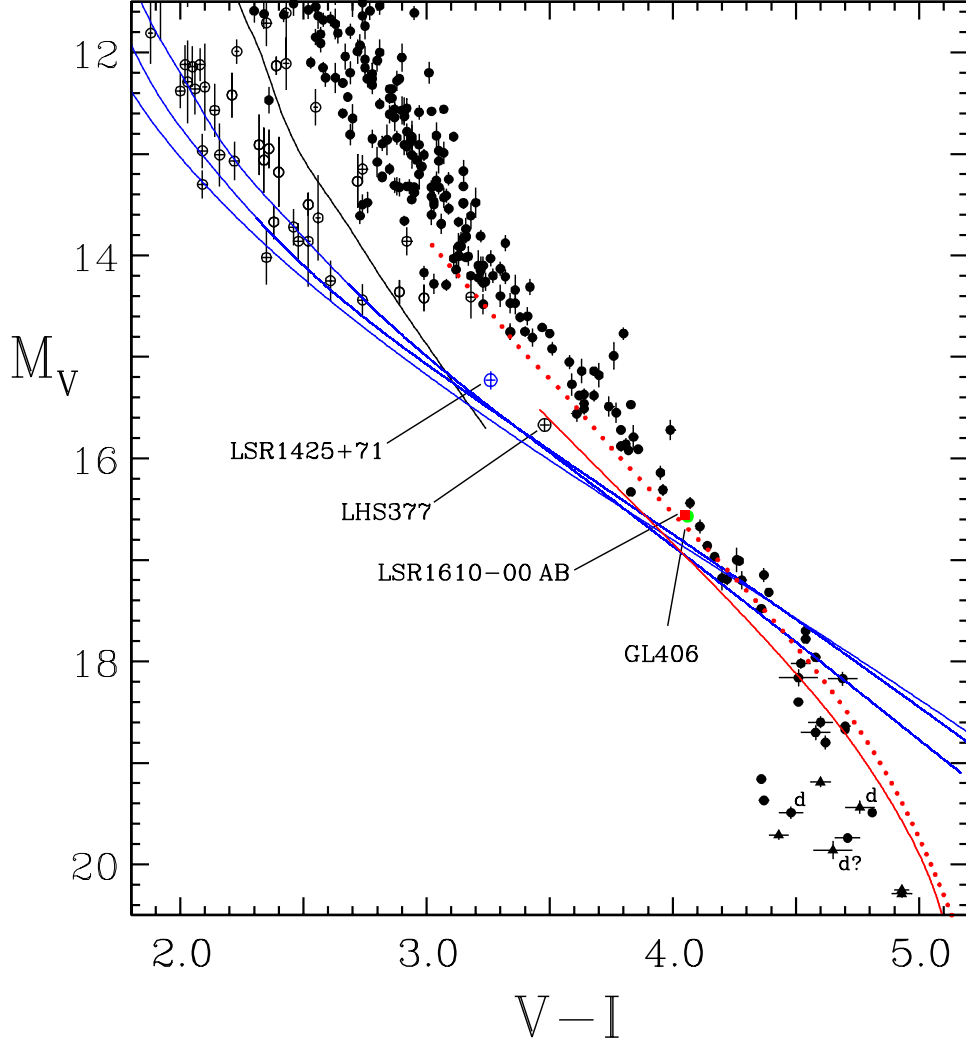


Fig. 2.— LSR1425+71 and LSR1610-00 in the M_V versus $V-I$ diagram. A selection of M-type dwarfs (solid circles), M-type subdwarfs (open circles), and early L-type dwarfs (solid triangles) are plotted for reference and comparison. The solid blue lines are the Baraffe et al. (1997) isochrones for metallicities of $[M/H] = -1.0, -1.5,$ and -2.0 for an age of 10 Gyrs. The solid black line is the isochrone for solar metallicity stars with masses $\geq 0.10 M_\odot$ and with ages of 0.5 Gyr from Baraffe et al. (1998). The solid red and dotted red lines represent the isochrones for DUSTY models from Chabrier et al. (2000) with masses $\leq 0.10 M_\odot$ and with ages of 0.5 Gyr and 0.1 Gyr, respectively. Three of the latest dwarfs plotted that are either known or suspected double stars are flagged with ‘d’ or ‘d?’. The two other labeled stars (LHS377 and GL406) are discussed in the text.

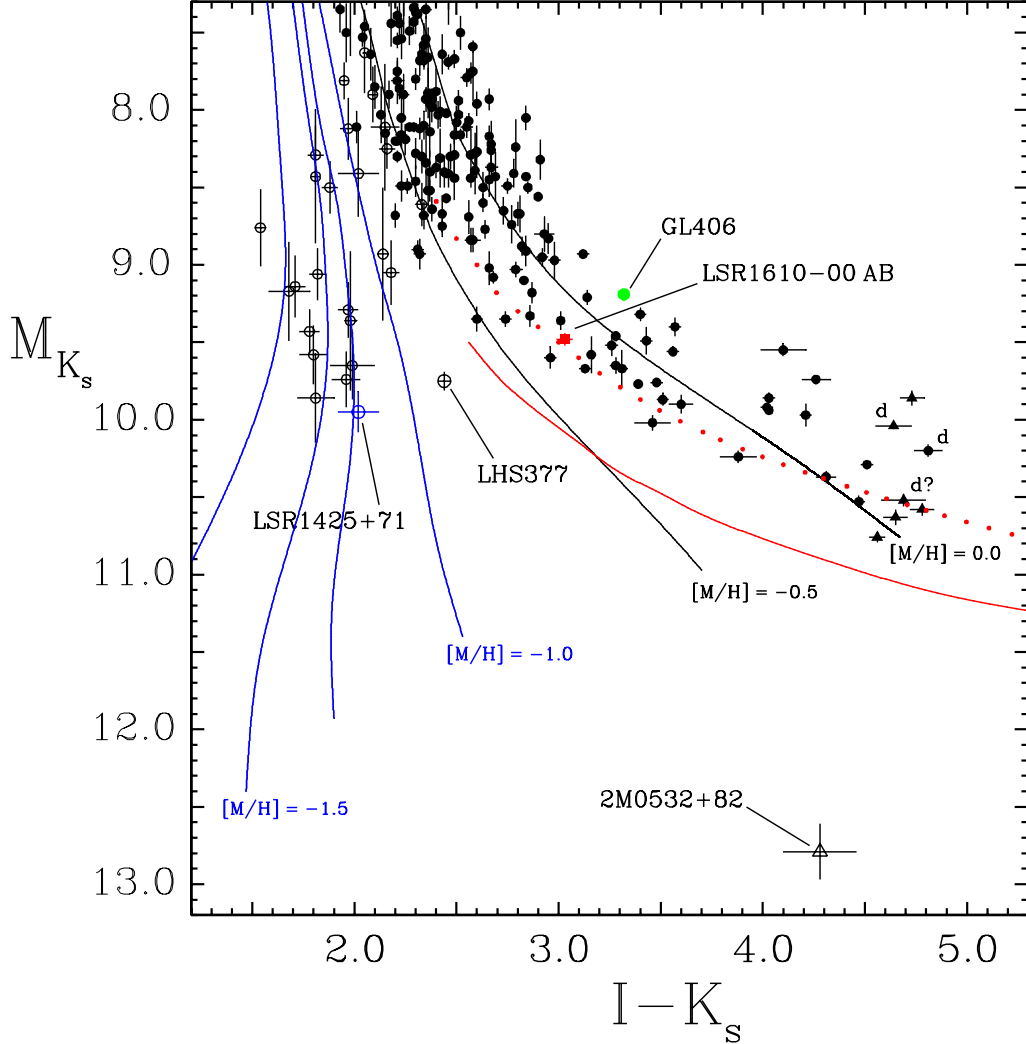


Fig. 3.— LRS1425+71 and LSR1610–00 in the M_{K_s} versus $I-K_s$ diagram. A selection of M-type dwarfs (solid circles), M-type subdwarfs (open circles), and early L-type dwarfs (solid triangles) are plotted for reference and comparison. The solid blue lines are the Baraffe et al. (1997) isochrones for metallicities of $[M/H] = -1.0, -1.3, -1.5,$ and -2.0 for an age of 10 Gyrs. The solid black lines are isochrones for solar metallicity and slightly metal-poor stars with masses $\geq 0.10 M_\odot$ and with ages of 0.5 Gyr from Baraffe et al. (1998). The solid red and dotted red lines represent the isochrones for DUSTY models from Chabrier et al. (2000) with masses $\leq 0.10 M_\odot$ and with ages of 0.5 Gyr and 0.1 Gyr, respectively. Three of the latest dwarfs plotted that are either known or suspected double stars are flagged with ‘d’ or ‘d?’. The three other labeled stars (LHS377, GL406, and 2M0532+82) are discussed in the text.

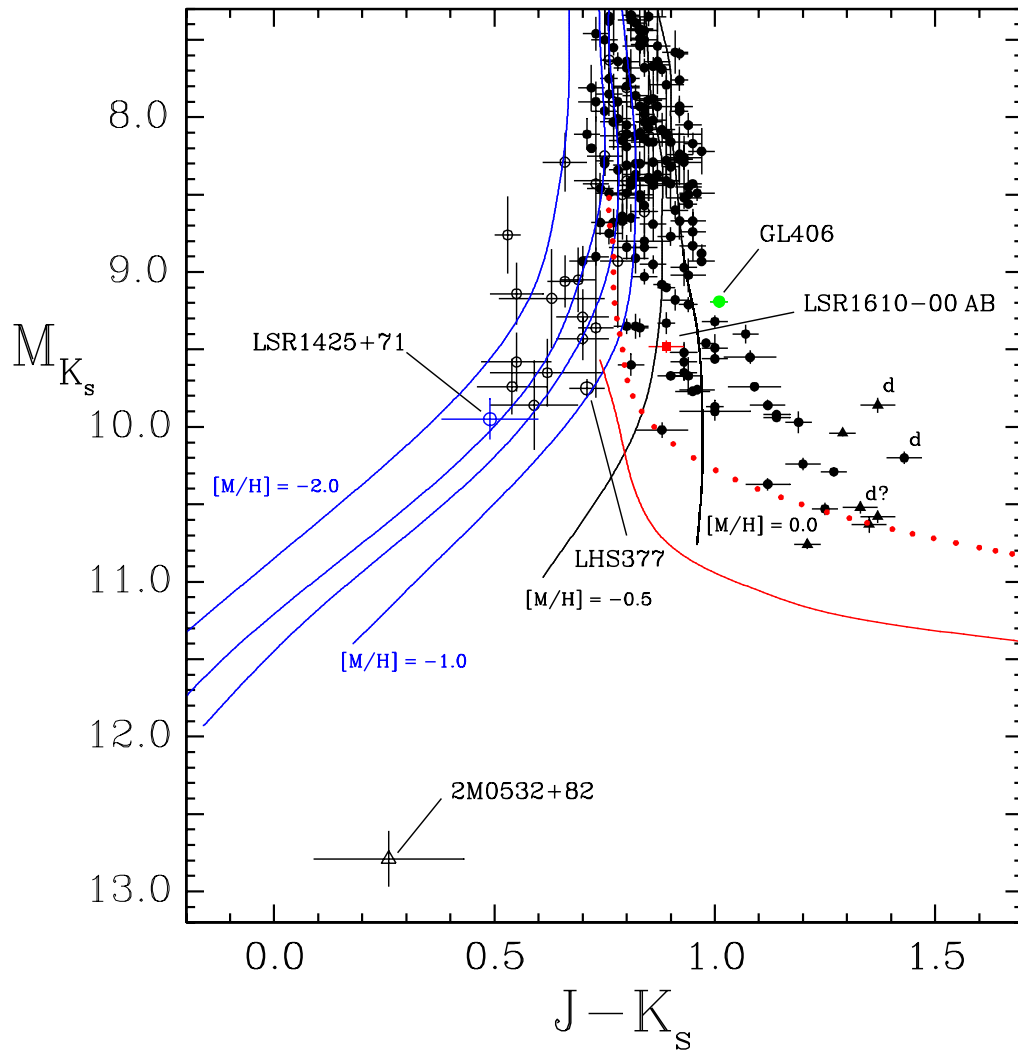


Fig. 4.— LRS1425+71 and LSR1610-00 in the M_{K_s} versus $J - K_s$ diagram. The symbols and isochrones shown are the same as in Fig. 3.

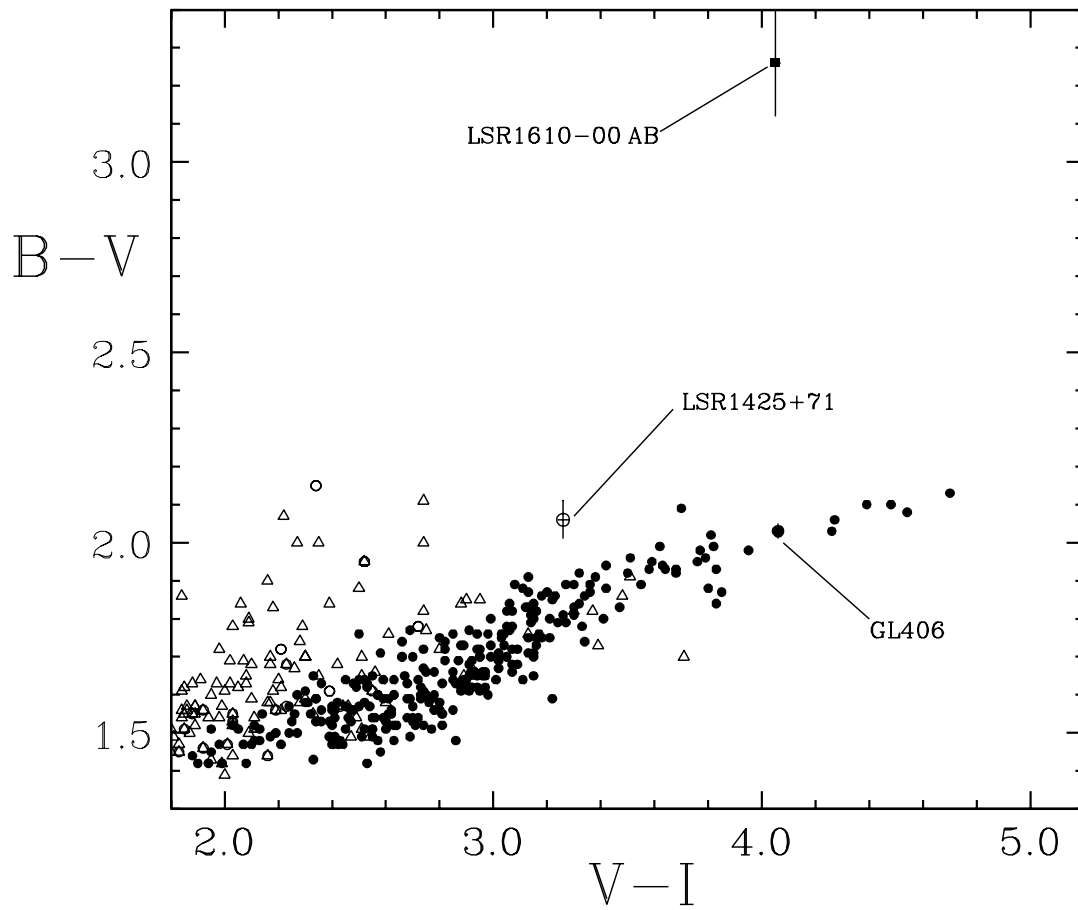


Fig. 5.— LSR1425+71, LSR1610–00AB, and GL406 in the $B-V$ versus $V-I$ diagram. Solid circles and open circles are M-type dwarfs and subdwarfs, respectively, as in Figure 2. Open triangles are stars spectroscopically classified as subdwarfs but lacking reliable parallax distances at this time.

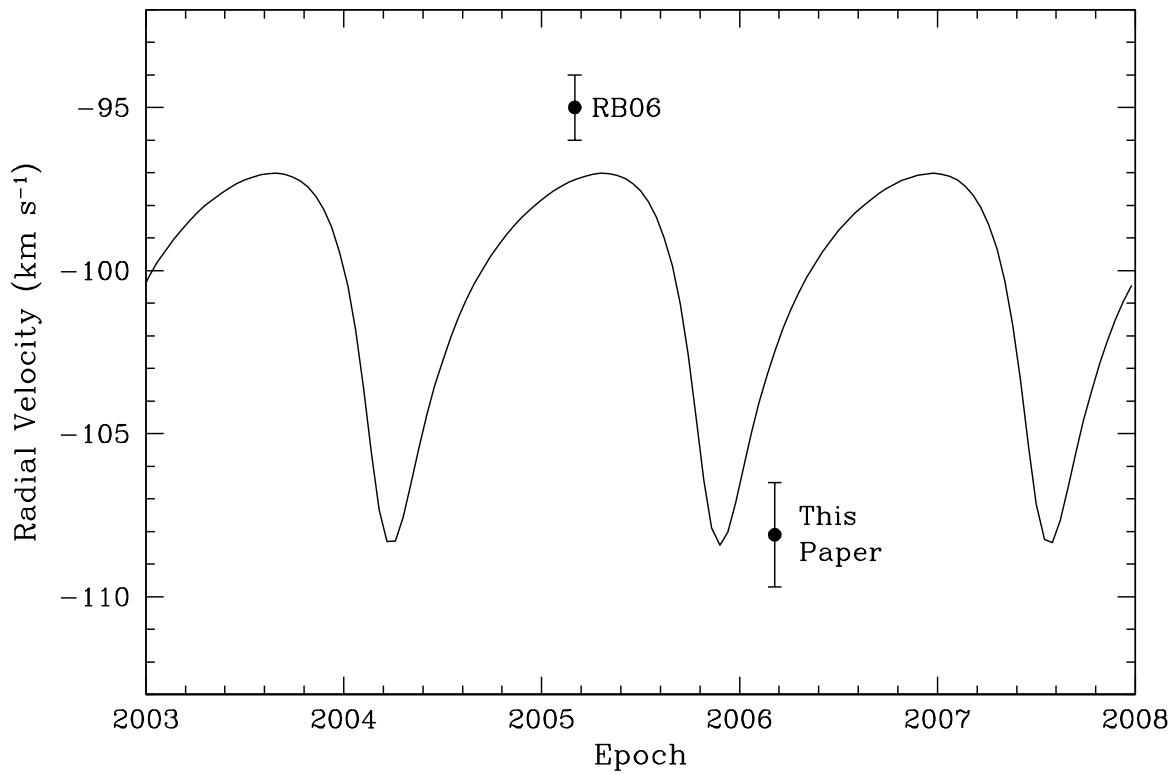


Fig. 6.— Heliocentric radial velocity observations of LSR1610–00 from RB06 and this paper, together with the orbital velocity curve predicted by the astrometric orbit with $\beta = 0$ (see text). The one other radial velocity observation by LRS03 has a large error and is not plotted.

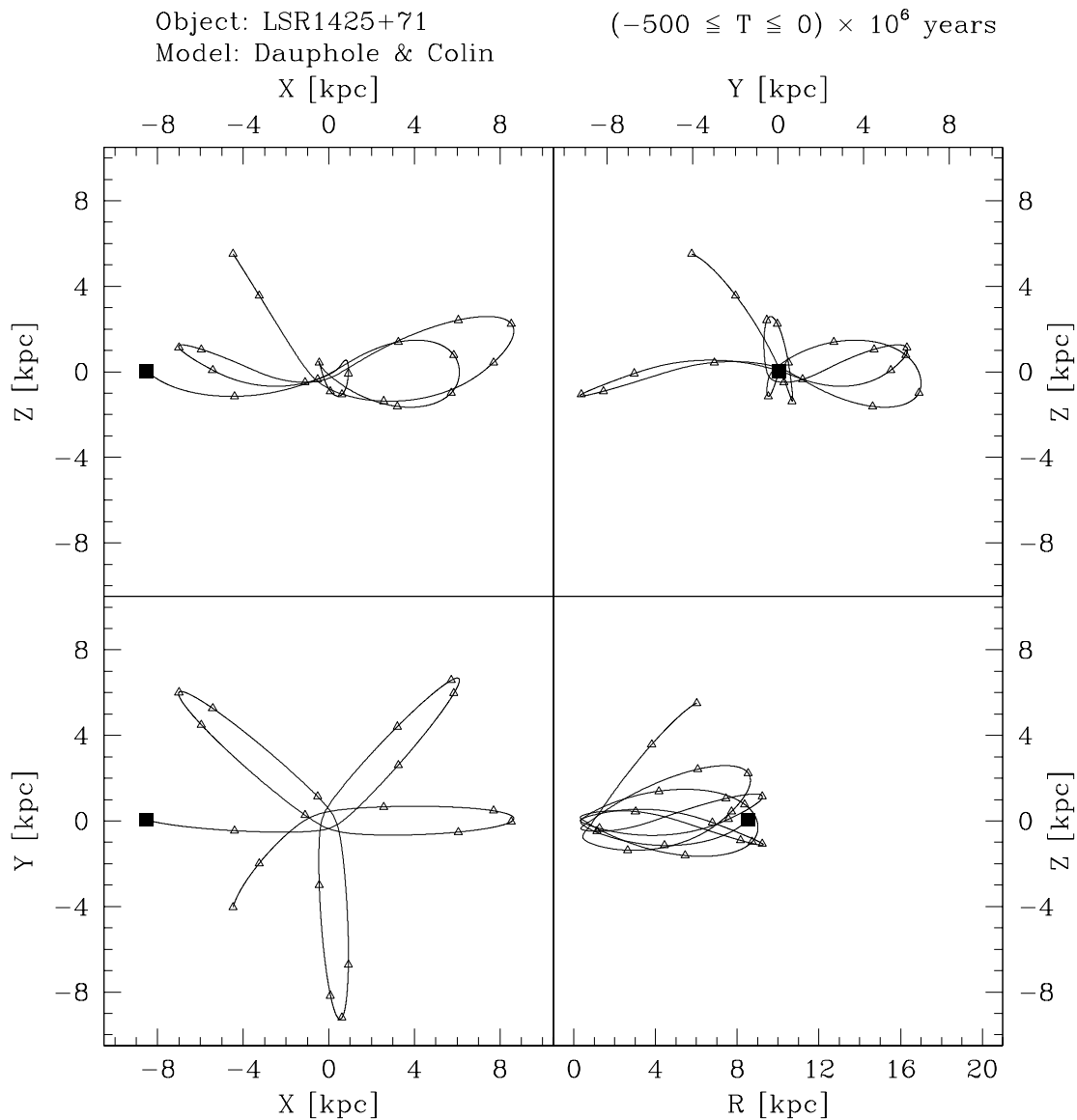


Fig. 7.— The $x-y$, $x-z$, $y-z$ and $R-z$ projections of the orbit of LSR1425+71 integrated backwards for 5×10^8 years in the Galactic model potential of Dauphole & Colin (1995). The filled square marks the star’s position now (and given the resolution, it also indicates the location of the solar neighborhood). The open triangles are placed at 25×10^6 year intervals.

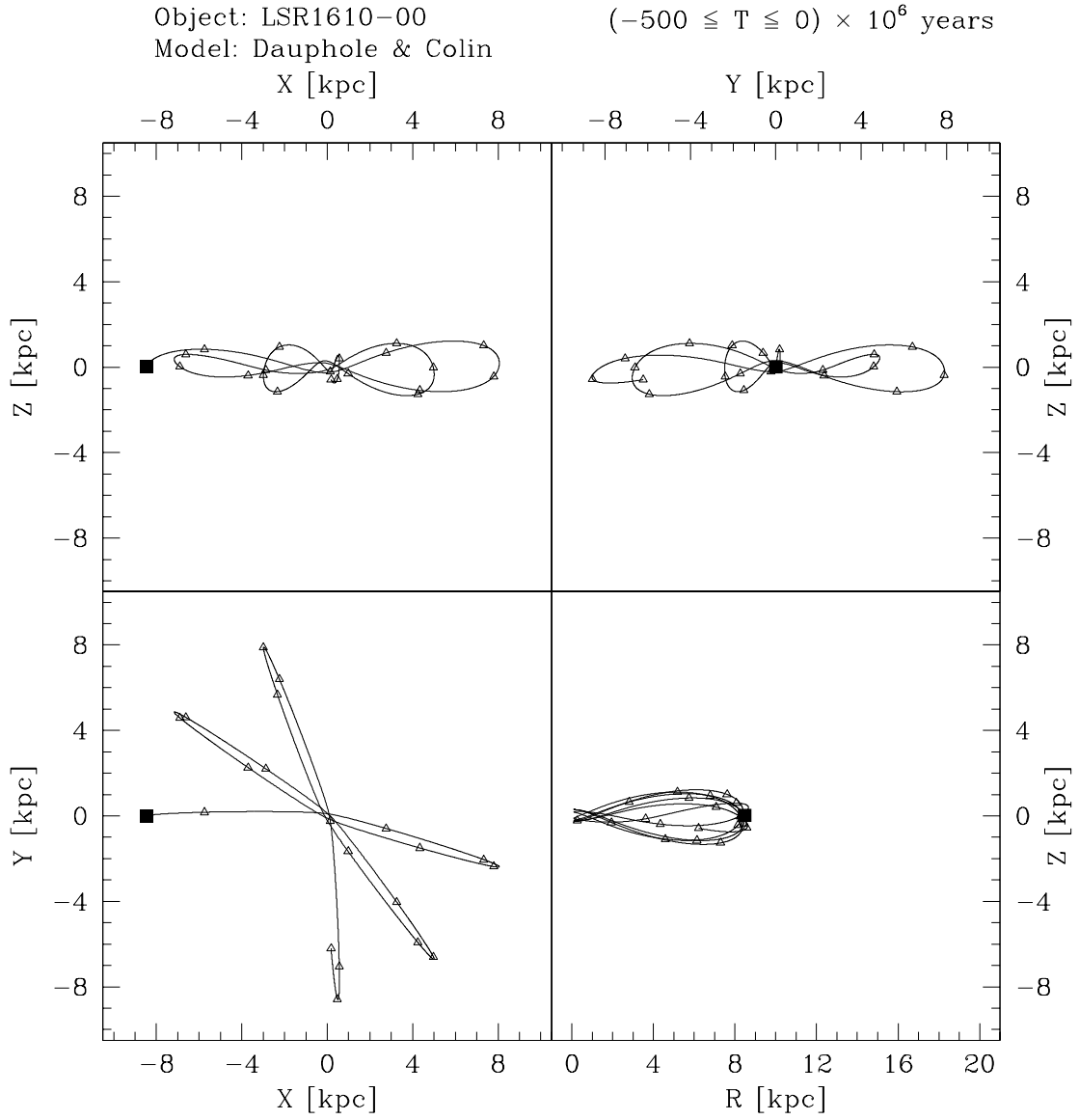


Fig. 8.— Projections of the orbit of LSR1610-00, where the panels and the symbols are the same as in Fig. 7.